

Polynomial Surrogate Training for Differentiable Ternary Logic Gate Networks

Sai Sandeep Damera
 Ryan Matheu
 Aniruddh G. Puranic
 John S. Baras

SDAMERA@UMD.EDU
 RMATHEU@UMD.EDU
 PURANIC@UMD.EDU
 BARAS@UMD.EDU

University of Maryland, College Park, MD, USA

Abstract

Differentiable logic gate networks (DLGNs) learn compact, interpretable Boolean circuits via gradient-based training, but all existing variants are restricted to the 16 two-input binary gates. Extending DLGNs to Ternary Kleene K_3 logic and training DTLGNs where the UNKNOWN state enables principled abstention under uncertainty is desirable. However, the support set of potential gates per neuron explodes to 19,683, making the established softmax-over-gates training approach intractable. We introduce *Polynomial Surrogate Training* (PST), which represents each ternary neuron as a degree-(2, 2) polynomial with 9 learnable coefficients (a $2,187\times$ parameter reduction) and prove that the gap between the trained network and its discretized logic circuit is bounded by a data-independent commitment loss that vanishes at convergence. Scaling experiments from 48K to 512K neurons on CIFAR-10 demonstrate that this hardening gap contracts with overparameterization. Ternary networks train 2-3 \times faster than binary DLGNs and discover true ternary gates that are functionally diverse. On synthetic and tabular tasks we find that the UNKNOWN output acts as a Bayes-optimal uncertainty proxy, enabling selective prediction in which ternary circuits surpass binary accuracy once low-confidence predictions are filtered. More broadly, PST establishes a general polynomial-surrogate methodology whose parameterization cost grows only quadratically with logic valence, opening the door to many-valued differentiable logic.

Keywords: Ternary Logic, Logic Gate Networks, Neuro-Symbolic AI.

1. Introduction

Logic gate networks replace conventional arithmetic neurons with compositions of discrete two-input logic gates, producing circuits that are inherently compact and interpretable (Petersen et al., 2022). Differentiable logic gate networks (DLGNs) make these circuits trainable through gradient descent by introducing continuous relaxations of the gate selection process. Since their introduction, DLGNs have been extended to convolutional architectures (Petersen et al., 2024), recurrent variants (Bühner et al., 2025), and connection-optimized formulations (Mommen et al., 2025), demonstrating competitive accuracy at extreme parameter efficiency.

All existing DLGNs share a common design: each two-input neuron maintains a softmax distribution over a fixed set of $K = 16$ Boolean gates, computes a weighted blend of their outputs during training, and selects a single gate via argmax at inference. This *softmax-over-gates* regime is viable precisely because the binary gate space is small enough to enumerate exhaustively. Yet it creates a structural train-test gap: the soft output $\sum_k p_k g_k(a, b)$ disagrees with the hard output $g_{k^*}(a, b)$ unless the softmax probability concentrates entirely on one gate. This is a degenerate limit with vanishing gradients. Concurrent work has proposed Gumbel-noise injection and straight-through estimation to mitigate this gap (Yousefi et al., 2025), though the fundamental issue with training cost remains unaddressed.

Why Ternary Logic? Binary DLGNs inherit the fundamental limitation of classical Boolean logic: every signal is either TRUE or FALSE, with no capacity to express uncertainty or indeterminate outcomes. Many tasks require exactly this capacity—classification under sensor dropout, temporal logic evaluation over finite observation windows, and medical diagnosis from incomplete records all demand *principled abstention*, where a network can output “not yet determined” rather than committing to an unsupported decision. Kleene’s strong three-valued logic K_3 (Kleene, 1952, 2002), with truth values $\mathcal{T} = \{-1, 0, +1\}$ representing FALSE, UNKNOWN, and TRUE, provides the minimal extension of Boolean logic that natively expresses this uncertainty. However, extending DLGNs to ternary logic reveals a fundamental limitation of the softmax-over-gates paradigm: a two-input ternary gate admits $3^2 = 19,683$ possible truth tables, making the categorical distribution approach intractable.

Polynomial Surrogate Training. We introduce PST, which replaces the categorical parameterization entirely: instead of learning a distribution over gates, each neuron learns the coefficients of a low-degree polynomial that directly represents a function over \mathcal{T}^2 . For ternary logic, this is a degree-(2, 2) polynomial with exactly 9 coefficients, reducing parameters by $2,187\times$ compared to softmax-over-gates while covering the full 19,683-gate vocabulary. PST is everywhere differentiable, requires no Gumbel tricks or softmax temperatures, and we prove that the per-neuron discretization error is bounded by a data-independent commitment loss (Theorem 1), providing a principled mechanism to narrow the train-test gap.

The hardening gap. While commitment regularization bounds per-neuron discretization error, activation quantization across layers creates network-level train-test mismatch. Empirically, this gap contracts with overparameterization, falling from 14.1pp to 3.7pp as scale increases from 96K to 512K neurons on CIFAR-10.

Fourier analysis on \mathcal{T}^2 . We develop a Fourier-analytic framework on $\{-1, 0, +1\}^n$ with an orthonormal basis appropriate for Kleene K_3 logic, including a quadratic term $\varphi_2(x) = x^2 - 2/3$ with no Boolean analogue that captures UNKNOWN-sensitivity. Fourier coefficients serve as spectral complexity measures for principled regularization and post-hoc analysis.

Contributions.

1. We introduce **Polynomial Surrogate Training (PST)**, the first training regime for logic gate networks that parameterizes the function space directly (9 coefficients per neuron for ternary logic) rather than through a distribution over gates. PST is everywhere differentiable and provides **provable bounds on the per-neuron hardening gap** via a data-independent commitment loss (Theorem 1).
2. We develop a **Fourier-analytic framework** on $\{-1, 0, 1\}^n$ with the orthogonal basis appropriate for Kleene K_3 logic, providing spectral characterization and principled regularization of learned gates.
3. Scaling experiments from 48K to 512K neurons on CIFAR-10 demonstrate PST trains ternary circuits 2-3 \times faster than binary DLGNs. On synthetic tasks, ternary circuits with UNKNOWN outputs achieve selective prediction, surpassing binary accuracy when low-confidence predictions are filtered.

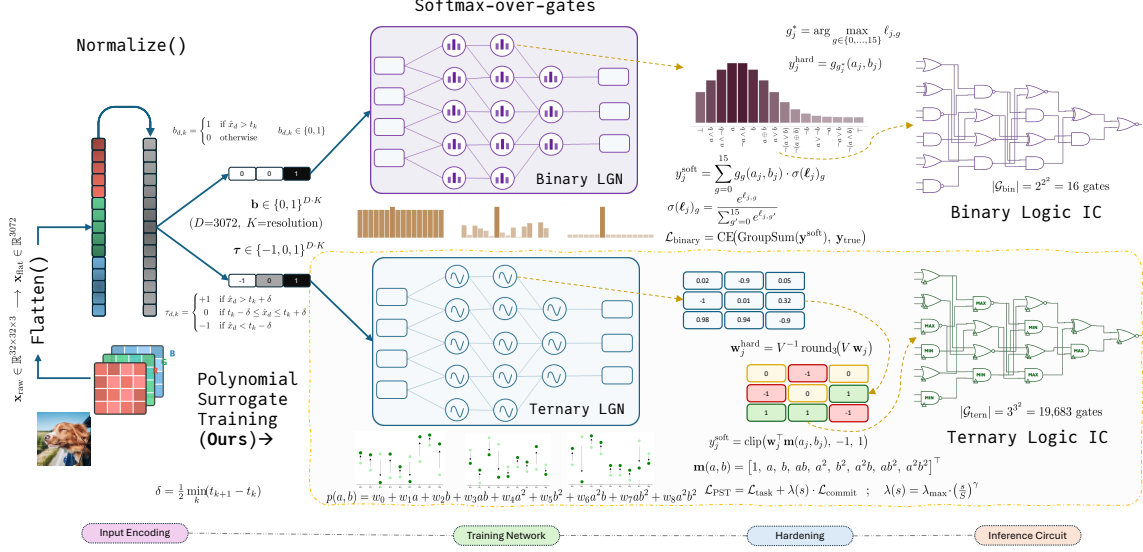


Figure 1: End-to-end comparison of binary DLGN training (top) and the proposed Polynomial Surrogate Training pipeline for ternary logic gate networks (bottom). **Input encoding** maps normalized features to bits/trits using temperature thresholding. **Training:** binary DLGNs learn softmax distributions over 16 gates per neuron; PST instead learns 9 polynomial coefficients per neuron, parameterising the full space of 19,683 ternary gates directly. **Hardening:** binary networks select the argmax gate; PST evaluates each polynomial on the 3×3 ternary grid, rounds to the nearest valid truth table, and recovers discrete gate coefficients via $w_j^{\text{hard}} = V^{-1} \text{round}_{\mathcal{T}}(V w_j)$. **Inference:** both pipelines produce logic circuits; which can be taped out as ultra-efficient ASICs for Inference

2. Related Work

Efficient Neural Architectures. The computational demands of deep neural networks have motivated efficient model design [Bengio et al. \(2013\)](#), including binary networks, sparse networks ([Frankle and Carbin, 2018](#)), and lookup-table approaches ([Zhu et al., 2016](#)). DLGNs reduce every computation to a two-input logic gate lookup. Weightless neural networks (WNNs) ([Susskind et al., 2022](#)) use arbitrary lookup tables, whereas PST neurons are constrained to encode *logic gates* with compositional semantics, enabling formal verification and spectral analysis.

Differentiable Logic Gate Networks Training networks of discrete components like logic gates is challenging because they are non-differentiable. [Petersen et al. \(2022\)](#) first introduced Differentiable Logic Gate Networks (DLGNs) to overcome this issue. Their approach relies relaxing discrete Boolean values $\{0, 1\}$ to continuous $[0, 1]$ and representing each of the 16 two-input gates as differentiable functions. Crucially, the learning does not involve selecting a single gate per neuron a priori. Instead, each neuron in a DLGN learns a categorical probability distribution over all 16 possible logic gates, computing a weighted blend during training and selecting the mode gate via argmax at inference to produce a discrete logic circuit. This final hardened network is a pure logic circuit, composed of fixed connections and discrete gates, making it extremely fast at inference and fully transparent. These networks can, in theory, be synthesized directly onto digital hardware for further speed, energy efficiency, and cybersecurity gains.

3. Background and Preliminaries

3.1. Polynomial Representations for Boolean Logic Functions

The mathematical foundation of PST rests on the fact that logic functions over finite domains have exact polynomial representations. Boolean functions admit exact real polynomial representations (Nisan and Szegedy, 1994; O’Donnell, 2014). Concretely, a real polynomial $p : \mathbb{R}^n \rightarrow \mathbb{R}$ is said to represent a Boolean function $f : \{-1, 1\}^n \rightarrow \{-1, 1\}$ if for all $x \in \{-1, 1\}^n$, $p(x) = f(x)$. Here we interpret TRUE as +1 and FALSE as -1. Because $z^{2k} = 1$, $z^{2k+1} = z$, $k \in \mathbb{N}$ for all $z \in \{-1, 1\}$, these polynomials are reduced to multi-linear polynomials. Let the set P_n contain all real multi-linear polynomials that represent Boolean functions with n inputs. Then (P_n, \cdot) is a finite abelian group with group multiplication “ \cdot ” defined as polynomial multiplication. This subtle notion allows for the definition of a Fourier expansion on representing polynomials, the details of which are described in Appendix D.

We extend this to the balanced ternary system with truth constants $\mathcal{T} = \{-1, 0, +1\}$ representing FALSE, UNKNOWN, and TRUE respectively. Analogous to the Boolean case, a real multivariate polynomial p is said to represent a ternary function of the form $f : \mathcal{T}^n \rightarrow \mathcal{T}$ if for all $x \in \mathcal{T}^n$, $p(x) = f(x)$. Consider $z \in \mathcal{T}$. For integer k odd, $k \geq 1$, $z^k = z$. For integer k even, $k \geq 2$, $z^k = z^2$. Therefore multivariate polynomials representing ternary functions are *multi-quadratic*, containing variables with powers no greater than two.

3.2. Fourier Analysis on \mathcal{T}

The monomial basis, while convenient for parameterization, is not orthogonal under the uniform inner product $\langle f, g \rangle = \frac{1}{3^n} \sum_{x \in \mathcal{T}^n} f(x) g(x)$. Consider the set of single input ($n = 1$) ternary functions of the form $f : \mathcal{T} \rightarrow \mathcal{T}$. Applying Gram-Schmidt orthogonalization to the basis $\{1, x, x^2\}$ yields the univariate orthogonal basis:

$$\varphi_0(x) = 1, \quad \varphi_1(x) = x, \quad \varphi_2(x) = x^2 - \frac{2}{3}.$$

The term φ_2 is the “centered quadratic”: it measures whether x is extreme (± 1 , where $\varphi_2(x) = \frac{1}{3}$) versus neutral (0, where $\varphi_2(x) = -\frac{2}{3}$). This basis function has no Boolean analogue—it captures the UNKNOWN-sensitivity that distinguishes Kleene K_3 from classical logic. The bivariate Fourier basis consists of the nine products $\{\varphi_i(x) \varphi_j(y)\}_{0 \leq i, j \leq 2}$, and the Fourier expansion of any $f : \mathcal{T}^2 \rightarrow \mathbb{R}$ is $f = \sum_{i, j} \hat{f}_{ij} \varphi_i \varphi_j$. The Fourier coefficients \hat{f}_{ij} serve as spectral complexity measures: the L_1 norm $\sum |\hat{f}_{ij}|$ quantifies gate complexity, and we use it as a regularizer during training to bias learning toward spectrally sparse (interpretable) gates. The full derivation is provided in Appendix B.

4. The Polynomial Surrogate Training Framework for DTLGNs

4.1. PST Formulation

The softmax-over-gates training regime creates an irreducible train-test gap: the soft network computes convex combinations of gate outputs while the hard network executes a single discrete gate. Gumbel relaxation approaches (Kim, 2023) and Straight Through Estimation techniques (Yousefi et al., 2025) reduce but do not eliminate this gap, and are intractable for ternary logic’s 19,683-gate support.

Our proposed Polynomial Surrogate Training (PST) regime addresses this gap by replacing the categorical parameterization with a direct polynomial parameterization. Each neuron learns a 9-coefficient polynomial $p_{\mathbf{w}} : \mathbb{R}^2 \rightarrow \mathbb{R}$ that approximates a ternary gate truth table on \mathcal{T}^2 , with per-neuron discretization error bounded by a commitment regularizer.

PST neuron. Each PST neuron represents a two-input ternary function as a degree-(2, 2) polynomial with 9 learnable coefficients $\mathbf{w} \in \mathbb{R}^9$:

$$p_{\mathbf{w}}(a, b) = \mathbf{w}^\top \mathbf{m}(a, b), \quad (1)$$

where $\mathbf{m}(a, b) = [1, a, b, ab, a^2, b^2, a^2b, ab^2, a^2b^2]^\top$ is the monomial basis. Since the 9×9 Vandermonde matrix \mathbf{V} evaluating this polynomial on \mathcal{T}^2 is invertible, the parameterization is universal: any function $f : \mathcal{T}^2 \rightarrow \mathbb{R}$ has a unique representation. The polynomial is C^∞ -smooth and linear in \mathbf{w} , requiring no softmax or Gumbel relaxations, and evaluates in 8 multiplications and 8 additions per neuron.

Network architecture. A PST-DTLGN is specified by its depth L , widths $\{n_l\}_{l=0}^L$, a connectivity map \mathbf{C} assigning two parent neurons to each neuron, and polynomial coefficients $\mathbf{w}_j^{(l)} \in \mathbb{R}^9$. The training forward pass applies a clip nonlinearity after each polynomial evaluation:

$$h_j^{(l)} = \text{clip}\left(p_{\mathbf{w}_j^{(l)}}(h_{s_j}^{(l-1)}, h_{t_j}^{(l-1)})\right), \quad (2)$$

where $\text{clip}(x) = \max(-1, \min(1, x))$. Clipping preserves the range $[-1, 1]$, prevents polynomial blowup across layers, preserves grid points $\{-1, 0, +1\}$ exactly, and implicitly regularizes toward ternary-range outputs through its zero-gradient saturation regime.

Initialization. Weights are drawn i.i.d. from $\mathcal{N}(0, 0.45^2)$, chosen to ensure $\text{Var}[p_{\mathbf{w}}(a, b)] \approx 1$ on ternary inputs, analogous to Xavier initialization (Glorot and Bengio, 2010).

4.2. Training

The training objective combines task loss with a commitment regularizer:

$$\mathcal{L}(\mathbf{W}) = \mathcal{L}_{\text{task}}(\mathbf{W}) + \lambda(t) \cdot \mathcal{R}_A(\mathbf{W}), \quad (3)$$

where $\mathbf{W} = \{\mathbf{w}_j^{(l)}\}$ is the set of all polynomial coefficients and the commitment loss is:

$$\mathcal{R}_A(\mathbf{W}) = \frac{1}{N} \sum_j \frac{1}{q^2} \sum_{(a,b) \in \mathcal{Q}^2} \text{dist}(p_{\mathbf{w}_j}(a, b), \mathcal{Q})^2, \quad (4)$$

with $\text{dist}(x, \mathcal{Q}) = \min_{v \in \mathcal{Q}} |x - v|$, where \mathcal{Q} is the set of q truth values. For ternary logic, $q = 3$ and $\mathcal{Q} = \{-1, 0, 1\}$. The regularization weight $\lambda(t) = \lambda_{\max}(t/T)^\gamma$ is annealed from ≈ 0 (free exploration) to λ_{\max} (strong commitment) using a scheduling regime.

4.3. Hardening: From Polynomials to Gates

At inference, each PST neuron is converted to a discrete ternary gate via Algorithm 1. Since rounding always produces a valid truth table in \mathcal{T}^9 , every trained PST neuron discretizes to one of the 19,683 possible two-input ternary gates without requiring a curated vocabulary—a fundamental advantage over the softmax regime, where the vocabulary must be fixed before training.

Algorithm 1 PST Neuron Hardening**Input:** Polynomial coefficients $\mathbf{w}_j \in \mathbb{R}^9$, Vandermonde matrix \mathbf{V} , gate library \mathcal{G} **Output:** Discrete gate $g_j^* : \mathcal{T}^2 \rightarrow \mathcal{T}$

```

 $\mathbf{t}_j \leftarrow \mathbf{V}\mathbf{w}_j$ ; // Evaluate polynomial at grid points  $\mathcal{T}^2$ 
 $\bar{\mathbf{t}}_j \leftarrow \text{round}_{\mathcal{T}}(\mathbf{t}_j)$ ; // Round each entry to nearest value in  $\mathcal{T}$ 
 $g_j^* \leftarrow \mathcal{G}[\bar{\mathbf{t}}_j]$ ; // Lookup gate in precomputed library
return  $g_j^*$ 

```

4.4. The Hardening Gap

Hardening converts the continuous training-time model into a discrete circuit by rounding each neuron’s polynomial to the nearest gate in the truth-table lattice $\Lambda_q = \mathcal{Q}^{q^2}$ (see Appendix A for lattice geometry). For ternary logic, this lattice has $3^9 = 19,683$ points in \mathbb{R}^9 .

Theorem 1 (PST Hardening Gap Bound) *Let \mathcal{N} be a q -logic PST network with N neurons. Let $\mathbf{t}_j = [p_{\mathbf{w}_j}(a, b)]_{(a,b) \in \mathcal{Q}^2}$ be neuron j ’s soft truth table and $\bar{\mathbf{t}}_j \in \Lambda_q$ its hardened truth table. Then*

$$\mathcal{R}_A(\mathbf{W}) = \frac{1}{N} \sum_{j=1}^N \frac{1}{q^2} \|\mathbf{t}_j - \bar{\mathbf{t}}_j\|_2^2.$$

Proof By Algorithm 1, hardening rounds each polynomial evaluation to the nearest value in \mathcal{Q} , so $\bar{t}_{j,(a,b)} = \arg \min_{v \in \mathcal{Q}} |p_{\mathbf{w}_j}(a, b) - v|$. Therefore $(p_{\mathbf{w}_j}(a, b) - \bar{t}_{j,(a,b)})^2 = \text{dist}(p_{\mathbf{w}_j}(a, b), \mathcal{Q})^2$. Summing over all grid points and averaging over neurons yields the result. ■

Remark 2 (Scaling and Data-Independence) *PST’s design improves with logic valence: a q -logic neuron requires only q^2 coefficients (vs. softmax’s super-exponential q^{q^2} logits) while achieving $O(1/q)$ rounding tolerance. The commitment loss \mathcal{R}_A is data-independent, so Theorem 1 holds for all inputs in \mathcal{Q}^n , not just the training distribution.*

5. Results

We evaluate PST on two fronts: scaling experiments demonstrating that ternary networks train efficiently at CIFAR-10 scale (Section 5.1), and analysis of principled abstention via UNKNOWN (U) outputs on synthetic tasks (Section 5.2). All models use JAX (Bradbury et al., 2018) with Equinox (Kidger and Garcia, 2021) and Adam. Binary DLGNs follow Petersen et al. (2022). Full details in Appendix C.

5.1. Training DTLGNs at scale using PST

We demonstrate that Polynomial Surrogate Training (PST) successfully trains differentiable ternary logic gate networks (TLGN) at CIFAR-10 scale, achieving soft accuracy parity with binary DLGNs while training 2–3× faster. The hardening gap (the accuracy cost of converting continuous polynomials to discrete ternary circuits) contracts from 14.1 pp to 3.7 pp as network scale increases from 96K to 512K neurons, establishing a clear trajectory toward gap elimination through overparameterization and commitment loss modulation.

Table 1: **Performance across all scales.** Soft: continuous forward pass (10K test). Circuit: post-hardening discrete evaluation (2K samples; ± 2.2 pp CI). Gap = Soft – Circuit. UNK%: fraction of TLGN output neurons producing zero (not sample-level abstention). Speed: DLGN/TLGN wall-time ratio (RTX 4090).

Model	Neurons	Soft Acc	Circuit Acc	Gap (pp)	UNK%	Speed
DLGN-SMALL	48K	49.3%	48.9%	+0.5	—	1.5×
TLGN-SMALL	48K	45.4%	42.6%	+2.8	5.9%	
DLGN-MEDIUM	96K	50.7%	51.4%	-0.8	—	2.0×
TLGN-MEDIUM	96K	50.3%	36.1%	+14.1	6.2%	
DLGN-LARGE	144K	51.4%	51.7%	-0.4	—	2.1×
TLGN-LARGE	144K	51.5%	38.5%	+13.0	6.0%	
DLGN-VLARGE	192K	51.6%	52.0%	-0.4	—	2.1×
TLGN-VLARGE	192K	51.2%	39.2%	+11.9	9.3%	
DLGN-HUGE	512K	52.5%	53.0%	-0.5	—	3.1×
TLGN-HUGE	512K	52.1%	48.4%	+3.7	24.6%	
DLGN-DEEPER	60K	49.3%	49.4%	-0.1	—	1.8×
TLGN-DEEPER	60K	45.0%	43.0%	+2.0	7.3%	

Setup. CIFAR-10 (50K train / 10K test) is flattened to 3,072 dimensions and encoded via resolution-4 balanced encoding ($K=3$ thresholds), producing 9,216 binary or ternary input features. We evaluate six homogeneous 4-layer architectures from SMALL ($4 \times 12K$ neurons, 48K total) to HUGE ($4 \times 128K$, 512K total), plus a 5-layer DEEPER variant (60K total); see Table 3 for full configurations. All share identical random sparse connectivity (seed = 42) with two inputs per neuron. Binary DLGN uses Adam ($\text{lr} = 0.01$), cross-entropy via GroupSum ($k=10$, $\tau=33.3$). Ternary PST uses Adam (lr adapted per scale), $\lambda_{\max}=0.1$, $\gamma=2.0$ (quadratic lambda annealing), MSE via GroupSum. Batch size 100 for both. Soft accuracy: full 10K test set; circuit accuracy: 2K samples (± 2.2 pp Wilson CI at $\sim 50\%$). Table 1 presents the central results across all scales.

PST trains ternary circuits at scale. Both architectures achieve comparable soft accuracy at all scales \geq MEDIUM, plateauing at $\sim 52\%$, a ceiling imposed by the resolution-4 encoding rather than network capacity. At HUGE: TLGN 52.1% vs. DLGN 52.5% ($p=0.57$, not significant). This parity is the key feasibility result: PST’s free polynomial parameterization (9 coefficients per neuron, searching 19,683 possible ternary gates) matches the representational capacity of the constrained softmax-over-16-gates approach, confirming that the ternary polynomial search space is trainable at scale.

The hardening gap closes with overparameterization. The PST hardening gap follows a non-monotonic trajectory: modest at SMALL (+2.8 pp), peaking at MEDIUM (+14.1 pp), then contracting steadily through LARGE (+13.0), VLARGE (+11.9), to HUGE (+3.7 pp). This contraction is accompanied by a $10\times$ reduction in per-neuron hardening error ($0.298 \rightarrow 0.029$) and a $4\times$ increase in U output neurons ($5.9\% \rightarrow 24.6\%$). For the neurons whose hardened truth tables map to zero, contributing no signal to the GroupSum class scores (a possibility unique to ternary circuits, where 0 is a valid output value). This indicates that overparameterization enables implicit pruning: poorly-committed

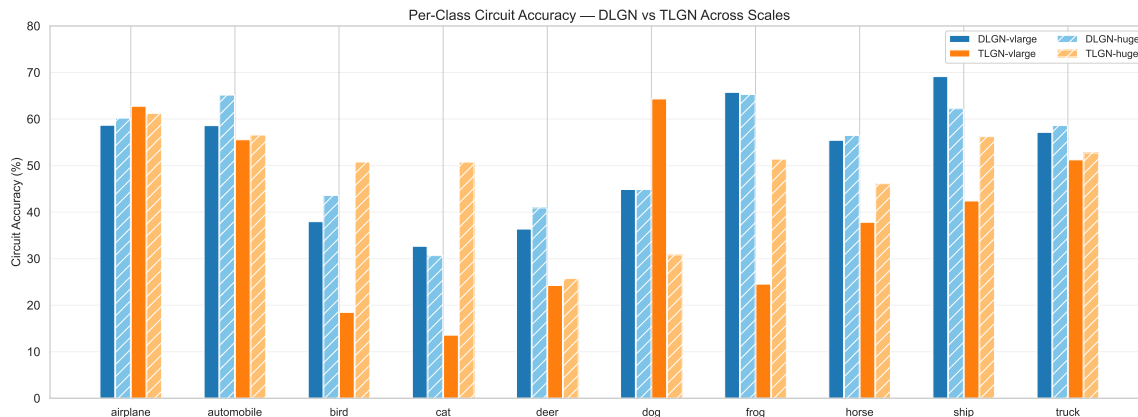


Figure 2: **Per-class circuit accuracy (vLARGE and HUGE)**. Blue: DLGN. Orange: TLGN. Solid: vLARGE. Hatched: HUGE. TLGN-HUGE recovers on visually complex classes (bird +32.3 pp, cat +37.2 pp, frog +26.9 pp vs. vLARGE), surpassing DLGN on bird and cat.

neurons are mapped to zero-output gates during hardening, while the surviving neurons are well-committed to valid ternary truth tables. The mechanism is detailed in §C.1.2; Figure 2 shows the per-class impact.

TLGNs train 2-3× faster. PST evaluates one polynomial per neuron (9 multiply-adds) vs. DLGN’s softmax over 16 gates, yielding 1.5× to 3.1× speedup across scales. PST matches binary DLGN soft accuracy while producing circuits whose hardening gap contracts with scale.

Takeaway. PST is a viable and efficient training regime for ternary logic gate networks. It matches binary DLGN soft accuracy, trains 2–3× faster, and produces circuits whose hardening gap contracts with scale. The intrinsic advantages of ternary logic (principled abstention via U outputs, a 500× richer gate vocabulary, and three-valued expressiveness) are examined in the following subsection.

5.2. Salient Features of Ternary LGNs

Binary logic gate networks (DLGN) must always commit to a classification: every neuron outputs $\{0, 1\}$, and the GroupSum aggregation always produces a decisive class score. Ternary logic gate networks (TLGN), by contrast, operate in $\{-1, 0, +1\}$, where zero propagates through truth-table lookup as a first-class signal. This three-valued logic endows the deployed circuit with principled abstention, selective prediction, and Bayes-tracking uncertainty. These capabilities have no analog in binary DLGNs and are only accessible via PST, the first training regime that makes ternary gate networks trainable.

We validate these properties on five 2D synthetic datasets (Moons, Circles, Spirals, Gaussians, Ring Sector; $n=2,000$ train, 500 test) using matched architectures: body $[512]^3$, output = 200, GroupSum($k=2$, $\tau=10.0$), resolution-4 encoding ($K=3$, input dim = 6). Both architectures are trained for 5,000 steps with discrete inputs.

Table 2: **Ternary vs. binary: accuracy, abstention, and selective prediction.** Δ : ternary – binary accuracy. UNK%: fraction of ternary output neurons producing zero. $\text{Acc}@k\%$: ternary accuracy when retaining only the $k\%$ most confident samples (binary has no analogous mechanism).

Dataset	Raw Accuracy			Ternary Selective Prediction			
	Bin	Tern	Δ	UNK%	Acc@90%	Acc@50%	AUC
Moons	91.8%	85.8%	−6.0	52.9%	90.2%	98.1%	−0.955
Circles	97.0%	78.2%	−18.8	45.1%	76.7%	84.9%	−0.864
Spirals	63.2%	64.2%	+1.0	50.1%	65.4%	78.2%	−0.790
Gaussians	90.5%	78.8%	−11.8	50.6%	78.8%	99.5%	−0.846
Ring Sector	97.0%	92.2%	−4.7	38.3%	96.9%	100.0%	−0.986

5.2.1. THE U SIGNAL: PRINCIPLED ABSTENTION ABSENT IN BINARY DLGNs

Table 2 presents the head-to-head comparison. Binary DLGN achieves higher raw accuracy on four of five datasets (+4.7 to +18.8 pp), but this comparison is misleading: the ternary circuit deliberately abstains on ambiguous inputs via its U mechanism, concentrating zero-valued outputs at decision boundaries (Figure 3). Under margin-based selective prediction, the ternary circuit surpasses binary full-coverage accuracy: at 50% coverage, Moons achieves 98.1% (vs. binary’s 91.8%), Gaussians 99.5%, and Ring Sector 100.0%. This demonstrates that ternary circuits provide more reliable predictions on inputs they choose to classify, a capability unavailable to binary circuits (see Appendix C.2.1–C.2.2 for full decision boundary gallery and accuracy-vs-coverage curves).

U as a Bayes-optimal uncertainty proxy To confirm that the U signal reflects genuine statistical uncertainty rather than training failure, we parametrically vary the difficulty of the Gaussian classification task (Appendix Table 10). As class separation increases from 0.5σ to 3.0σ , three quantities decrease together: the Bayes error, the ternary U fraction, and the spatial overlap between U density and the Bayes entropy $H(y | x)$ (Figure 3). The binary baseline matches the Bayes rate at every separation level, confirming that these tasks are within both architectures’ capacity. The ternary circuit trades coverage for accuracy in precisely the regions where the Bayes posterior is ambiguous, a behavior that emerges naturally from the three-valued signal domain without any explicit calibration objective.

5.2.2. PST DELIVERS TERNARY CIRCUITS WITH NEAR-ZERO HARDENING GAP

The practical value of these ternary-specific features depends on whether PST can faithfully transfer the trained behavior to the deployed circuit. Table 2 includes the hardening gap ($|\text{soft} - \text{circuit}|$) for both architectures: the binary gap is 0.00% on four of five datasets (3.19% on Spirals); the ternary gap is 0.00% on Moons, 0.31% on Gaussians, and 0.38% on Ring Sector. These near-zero gaps confirm that the polynomial surrogate training regime, including quadratic lambda annealing and ternary commitment regularization, produces circuits that preserve the training-time abstention behavior after hardening. The elevated ternary gaps on Circles (8.31%) and Spirals (4.31%) are consistent with the narrow hardening basins identified in the loss landscape analysis (Appendix Figure 13).

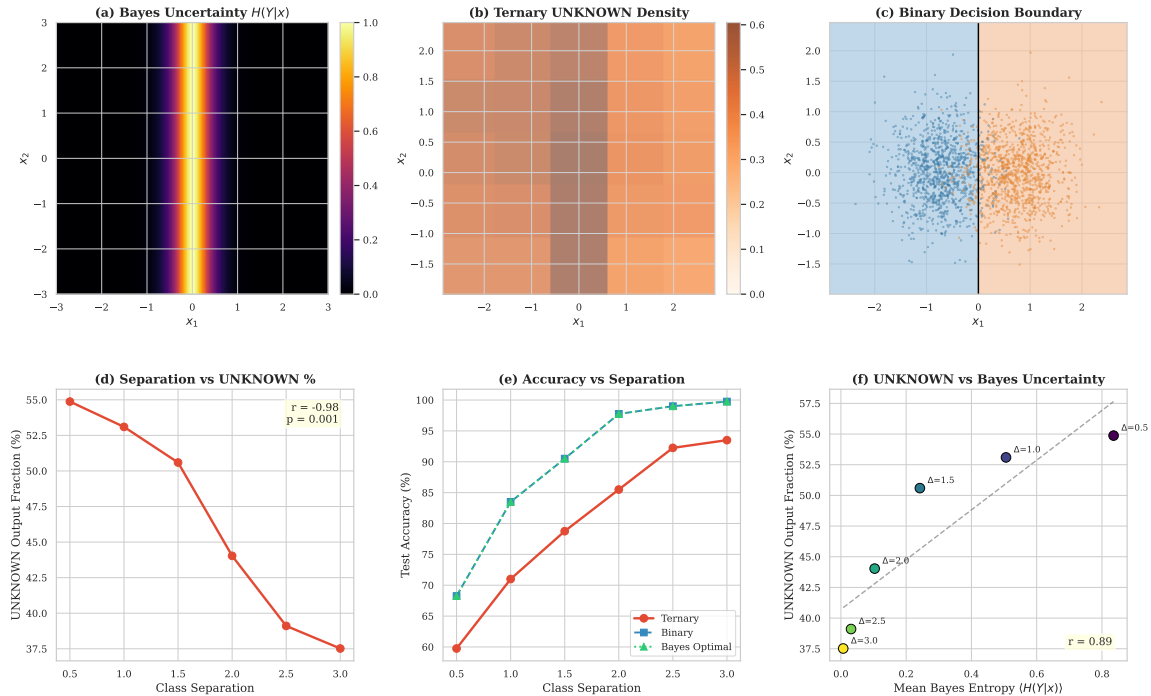


Figure 3: **Ternary U tracks Bayes-optimal uncertainty.** Top row: Bayes posterior entropy, ternary U density, and their overlay for Gaussians (separation = 1.5). Bottom row: as class separation increases from 0.5 to 3.0σ , U fraction and Bayes error decrease in lockstep. Binary accuracy (red) matches the Bayes rate at every separation, confirming that neither architecture is capacity-limited; the ternary circuit *chooses* to abstain where the posterior is ambiguous.

6. Conclusion and Future Work

We introduced Polynomial Surrogate Training (PST), which makes ternary logic gate networks practical by parameterizing the full 19,683-gate vocabulary with just 9 coefficients per neuron. PST provides provable bounds on per-neuron discretization error through a data-independent commitment loss and trains ternary circuits 2–3 \times faster than binary DLGNs. Ternary logic’s key advantage is principled abstention via UNKNOWN outputs, which enables selective prediction where circuits surpass binary accuracy by filtering low-confidence predictions: ternary circuits achieve 98.1% accuracy at 50% coverage (vs. 91.8% binary full-coverage accuracy on Moons), with UNKNOWN density tracking Bayes-optimal uncertainty across varying task difficulty, demonstrating that three-valued logic is a practical mechanism for uncertainty-aware inference in deployed circuits.

Two directions warrant immediate attention: (a) adapting straight-through estimation and Gumbel-noise regularization (Bengio et al., 2013; Yousefi et al., 2025) to PST’s polynomial regime may further narrow the network-level hardening gap that contracts empirically with scale but lacks theoretical guarantees; and, (b) extending PST to recurrent architectures would enable online temporal monitoring with three-valued logic, as Signal Temporal Logic (STL) specifications inherently require ternary verdicts (TRUE, FALSE, UNKNOWN) over finite observation windows, making recurrent DTLGNs a natural fit for runtime verification in safety-critical systems where partial observations demand principled abstention rather than forced binary classification.

References

- Yoshua Bengio, Nicholas Léonard, and Aaron Courville. Estimating or propagating gradients through stochastic neurons for conditional computation. *arXiv preprint arXiv:1308.3432*, 2013.
- James Bradbury, Roy Frostig, Peter Hawkins, Matthew James Johnson, Chris Leary, Dougal Maclaurin, George Necula, Adam Paszke, Jake VanderPlas, Skye Wanderman-Milne, and Qiao Zhang. JAX: composable transformations of Python+NumPy programs, 2018. URL <http://github.com/jax-ml/jax>.
- Simon Bühner, Andreas Plesner, Till Aczel, and Roger Wattenhofer. Recurrent deep differentiable logic gate networks. *arXiv preprint arXiv:2508.06097*, 2025.
- Jonathan Frankle and Michael Carbin. The lottery ticket hypothesis: Finding sparse, trainable neural networks. *arXiv preprint arXiv:1803.03635*, 2018.
- Xavier Glorot and Yoshua Bengio. Understanding the difficulty of training deep feedforward neural networks. In Yee Whye Teh and Mike Titterton, editors, *Proceedings of the Thirteenth International Conference on Artificial Intelligence and Statistics*, volume 9 of *Proceedings of Machine Learning Research*, pages 249–256, Chia Laguna Resort, Sardinia, Italy, 13–15 May 2010. PMLR. URL <https://proceedings.mlr.press/v9/glorot10a.html>.
- Douglas W Jones. The ternary manifesto. 2012. URL <https://homepage.cs.uiowa.edu/~jones/ternary/>.
- Patrick Kidger and Cristian Garcia. Equinox: neural networks in JAX via callable PyTrees and filtered transformations. *Differentiable Programming workshop at Neural Information Processing Systems 2021*, 2021.
- Youngsung Kim. Deep stochastic logic gate networks. *IEEE Access*, 11:122488–122501, 2023. doi: 10.1109/ACCESS.2023.3328622.
- Stephen Cole Kleene. Introduction to metamathematics. 1952.
- Stephen Cole Kleene. *Mathematical logic*. Courier Corporation, 2002.
- Roy D Merrill Jr. Ternary logic in digital computers. In *Proceedings of the SHARE design automation project*, pages 6–1, 1965.
- Wout Mommen, Lars Keuninckx, Matthias Hartmann, and Piet Wambacq. A method for optimizing connections in differentiable logic gate networks. *arXiv preprint arXiv:2507.06173*, 2025.
- Noam Nisan and Mario Szegedy. On the degree of boolean functions as real polynomials. *Computational complexity*, 4(4):301–313, 1994.
- Ryan O’Donnell. *Analysis of boolean functions*. Cambridge University Press, 2014.
- Felix Petersen, Christian Borgelt, Hilde Kuehne, and Oliver Deussen. Deep differentiable logic gate networks. *Advances in Neural Information Processing Systems*, 35:2006–2018, 2022.

Felix Petersen, Hilde Kuehne, Christian Borgelt, Julian Welzel, and Stefano Ermon. Convolutional differentiable logic gate networks. *Advances in Neural Information Processing Systems*, 37:121185–121203, 2024.

Zachary Susskind, Aman Arora, Igor DS Miranda, Luis AQ Villon, Rafael F Katopodis, Leandro S De Araújo, Diego LC Dutra, Priscila MV Lima, Felipe MG França, Mauricio Breternitz Jr, et al. Weightless neural networks for efficient edge inference. In *Proceedings of the International Conference on Parallel Architectures and Compilation Techniques*, pages 279–290, 2022.

Audrey Terras. *Fourier Analysis on Finite Groups and Applications*. Number 43 in London Mathematical Society Student Texts. Cambridge University Press, 1999.

Shakir Yousefi, Andreas Plesner, Till Aczel, and Roger Wattenhofer. Mind the gap: Removing the discretization gap in differentiable logic gate networks. *arXiv preprint arXiv:2506.07500*, 2025.

Chenzhuo Zhu, Song Han, Huizi Mao, and William J Dally. Trained ternary quantization. *arXiv preprint arXiv:1612.01064*, 2016.

Appendix A. Hardening Gap: Lattice Geometry

A.1. Truth-Table Lattice Quantization

Both the softmax-over-gates and PST training regimes face the same geometric problem: after training, each neuron must be assigned one of finitely many discrete gates. We formalize this as a quantization problem on a truth-table lattice.

Definition 3 (Truth-Table Lattice) *Let $\mathcal{Q} = \{v_0, v_1, \dots, v_{q-1}\} \subset \mathbb{R}$ be an equally spaced set of q truth values. The truth-table lattice $\Lambda_q = \mathcal{Q}^{q^2}$ is the set of all valid truth tables for two-input q -logic gates, embedded in \mathbb{R}^{q^2} . The lattice has $|\Lambda_q| = q^{q^2}$ points.*

For the cases of interest: Boolean logic has $q = 2$, $|\Lambda_2| = 2^4 = 16$ gates in \mathbb{R}^4 ; ternary logic has $q = 3$, $|\Lambda_3| = 3^9 = 19,683$ gates in \mathbb{R}^9 ; and quaternary logic has $q = 4$, $|\Lambda_4| = 4^{16} \approx 4.3 \times 10^9$ gates in \mathbb{R}^{16} .

Hardening maps each neuron’s continuous output (a point in \mathbb{R}^{q^2}) to the nearest lattice point in Λ_q . The per-neuron *hardening error* is the ℓ_2 distance from the neuron’s soft truth table to the nearest valid gate. The key geometric quantity is the *covering radius* of Λ_q : the maximum distance from any point in the ambient space to the nearest lattice point.

Proposition 4 (Covering Radius) *The covering radius of the lattice Λ_q (with truth values uniformly spaced by $\Delta = 2/(q - 1)$ in $[-1, 1]$) satisfies*

$$r_{\text{cov}}(\Lambda_q) = \frac{q}{q - 1},$$

and the maximum per-entry rounding error is

$$\epsilon_q = \frac{1}{q - 1}.$$

Proof Each coordinate of the truth table independently rounds to the nearest value in \mathcal{Q} . With q uniformly spaced values in $[-1, 1]$, consecutive values are separated by $\Delta = 2/(q - 1)$. The worst-case per-coordinate error is $\Delta/2 = 1/(q - 1)$. The ℓ_2 covering radius over all q^2 coordinates is $\sqrt{q^2 \cdot (\Delta/2)^2} = q \cdot \Delta/2 = q/(q - 1)$. ■

For ternary logic ($q = 3$), $\epsilon_3 = 1/2 = 0.5$; for quaternary ($q = 4$), $\epsilon_4 = 1/3 \approx 0.333$. As q increases, each coordinate need only be accurate to within $O(1/q)$ to snap to the correct gate entry.

Proposition 5 (PST Architectural Scaling) *A q -logic PST neuron over two inputs requires q^2 learnable coefficients. The maximum per-entry rounding error at hardening time is $\epsilon_q = 1/(q - 1) = O(1/q)$. Therefore, a higher-valence PST architecture achieves tighter rounding tolerance per truth-table entry at a cost that grows only quadratically in q . By contrast, a softmax-over-gates neuron for q -ary logic requires $K = q^{q^2}$ logits (super-exponential in q), and its rounding error is governed by the concentration of a categorical distribution over K categories.*

PST’s design improves with logic valence: the polynomial representation cost grows polynomially (q^2 coefficients) while the lattice becomes denser ($\epsilon_q \rightarrow 0$). The softmax-over-gates regime faces the opposite situation: its parameterization cost explodes super-exponentially while the concentration problem worsens.

Appendix B. Spectral Analysis of Ternary Logic Gate Networks

Computing the Orthonormal Basis. We have the ternary set $\mathcal{T} = \{-1, 0, +1\}$ and want to represent every function $f : \mathcal{T}^2 \rightarrow \mathbb{R}$ as a linear combination of basis functions. Since $|\mathcal{T}^2| = 9$, the space of such functions is \mathbb{R}^9 – nine-dimensional. We need exactly 9 basis functions, and we want them orthogonal under some inner product.

The Inner Product. The uniform measure on \mathcal{T} assigns probability $1/3$ to each value. The inner product on functions $f, g : \mathcal{T} \rightarrow \mathbb{R}$ is:

$$\langle f, g \rangle = \frac{1}{3} \sum_{x \in \mathcal{T}} f(x)g(x) = \frac{1}{3} [f(-1)g(-1) + f(0)g(0) + f(1)g(1)]$$

Each ternary input is equally weighted. The factor $1/3$ is a normalization - it makes $\langle 1, 1 \rangle = 1$ so the constant function has unit norm. The bivariate inner product on \mathcal{T}^2 uses the same idea with factor $1/9$.

The Monomial Basis. The monomials $\{1, x, x^2\}$ are a valid basis for polynomials of degree ≤ 2 in one variable, and they span the right space (any function $\mathcal{T} \rightarrow \mathbb{R}$ is determined by 3 values, and 3 monomials give 3 degrees of freedom). But they are not orthogonal under this inner product:

$$\langle 1, x^2 \rangle = \frac{1}{3} [1 \cdot 1 + 1 \cdot 0 + 1 \cdot 1] = \frac{2}{3} \neq 0$$

The constant function and x^2 are correlated on \mathcal{T} because x^2 evaluates to 1 at both ± 1 and 0 at 0 . Under the uniform measure, x^2 has mean $2/3$ - it is biased toward 1 because two out of three ternary inputs are extreme (± 1) and only one is neutral (0). Since x^2 is nonzero at two-thirds of the domain, its mean is nonzero, which means it is not orthogonal to the constant. The monomial basis is fine for computation (and is what we use for the weight parameterization), but it is unsuitable for analysis because the coefficients are entangled and we cannot ascribe meaning to the values of these coefficients like we can with the Fourier coefficients.

Gram-Schmidt Orthogonalization. We generate the orthonormal basis from the monomial basis by following the Gram-Schmidt process:

Step 1: $\varphi_0(x) = 1$. Norm: $\|\varphi_0\|^2 = \langle 1, 1 \rangle = 1$.

Step 2: Start with x , subtract its projection onto φ_0 .

$$\langle x, \varphi_0 \rangle = \frac{1}{3} (-1 \cdot 1 + 0 \cdot 1 + 1 \cdot 1) = 0$$

The projection is zero; x is already orthogonal to the constant. This happens because x is an odd function and the measure is symmetric around 0. So $\varphi_1(x) = x$, with $\|\varphi_1\|^2 = 2/3$.

Step 3: Start with x^2 , subtract projections onto φ_0 and φ_1 .

$$\langle x^2, \varphi_1 \rangle = \frac{1}{3} \left((-1)^2(-1) + 0^2 \cdot 0 + 1^2 \cdot 1 \right) = 0$$

Zero by symmetry $-x^2$ is even, x is odd, their product is odd, and odd functions sum to zero on \mathcal{T} . So we only need to subtract the φ_0 projection:

$$\begin{aligned}\langle x^2, \varphi_0 \rangle &= \frac{1}{3}(1 + 0 + 1) = \frac{2}{3} \\ \varphi_2(x) &= x^2 - \frac{\langle x^2, \varphi_0 \rangle}{\|\varphi_0\|^2} \cdot \varphi_0 = x^2 - \frac{2/3}{1} \cdot 1 = x^2 - \frac{2}{3}\end{aligned}$$

The $-2/3$ is not arbitrary - it is the mean of x^2 under the uniform measure on \mathcal{T} . The polynomial $\varphi_2(x) = x^2 - 2/3$ is the “centered” quadratic: it measures whether x is extreme (± 1 , where $\varphi_2 = 1/3$) versus neutral (0, where $\varphi_2 = -2/3$). It has zero mean on \mathcal{T} by construction with $\|\varphi_2\|^2 = 2/9$. In Boolean analysis on $\{-1, +1\}$, every function of one variable is a linear combination of 1 and x - there are only two basis functions because $|\{-1, +1\}| = 2$. The quadratic φ_2 is the “extra dimension” that ternary logic provides, and it captures exactly the UNKNOWN-sensitivity that makes Kleene K3 logic different from Boolean logic.

Remark 6 *Our basis differs from the additive-combinatorial convention in two ways: (i) we use real-valued orthogonal polynomials rather than complex characters, matching the real polynomial parameterization of PST neurons; and (ii) we construct the basis via Gram-Schmidt from $\{1, x, x^2\}$ rather than from the group characters of \mathbb{Z}_3 , yielding a basis that is adapted to the Kleene interpretation where $\{-1, +1\}$ are “decided” values and 0 is “undetermined.” The resulting quadratic basis function $\varphi_2 = x^2 - 2/3$ is orthogonal to both the constant and linear terms and captures precisely the sensitivity to UNKNOWN that has no analogue in Boolean Fourier analysis.*

The full list of the Fourier coefficients is as follows: $\Phi_{00} = 1, \Phi_{10} = x, \Phi_{01} = y, \Phi_{11} = xy, \Phi_{20} = x^2 - 2/3, \Phi_{02} = y^2 - 2/3, \Phi_{21} = (x^2 - 2/3)y, \Phi_{12} = x(y^2 - 2/3), \Phi_{22} = (x^2 - 2/3)(y^2 - 2/3)$.

Spectral complexity classes. The Fourier spectrum naturally stratifies the 19,683 ternary gates into complexity classes. **Linear gates** have energy only in $\hat{f}_{00}, \hat{f}_{10}, \hat{f}_{01}$. These include MAJORITY and the trivial pass-through gates, and they are the only gates that can be computed by a single linear threshold on ternary inputs. **Bilinear gates** additionally use the interaction term \hat{f}_{11} ; AND, OR, XOR, and their variants fall here. **Quadratic gates** involve \hat{f}_{20} or \hat{f}_{02} and are the genuinely “ternary” gates that distinguish between decided and undecided inputs. **Full gates** use all nine terms. The Fourier L_1 norm $\|\hat{f}\|_1 = \sum_{ij} |\hat{f}_{ij}|$ is a rigorous complexity measure: it upper-bounds the number of random examples needed to learn the gate to constant accuracy, and it determines the gate’s sensitivity to random input perturbations.

Fourier sparsity regularization. The L_1 norm of Fourier coefficients serves as a sparsity regularizer independent of the commitment loss:

$$\mathcal{R}_F(\mathbf{W}) = \frac{1}{N} \sum_{j=1}^N \sum_{i,k} |\hat{f}_{ik}^{(j)}|. \quad (\text{B.1})$$

The commitment loss \mathcal{R}_A drives neurons toward *any* of the 19,683 gates; the Fourier regularizer biases that choice toward spectrally sparse, interpretable gates. The combined training objective is $\mathcal{L} = \mathcal{L}_{\text{task}} + \lambda(t) \cdot \mathcal{R}_A + \beta \cdot \mathcal{R}_F$.

Table 3: **Architecture configurations.** All use GroupSum($k=10$, $\tau=33.3$) for 10-class output. Input dimension: 9,216.

Scale	Widths	Neurons	PST LR	Steps
SMALL	[12000, 12000, 12000, 12000]	48,000	0.003	100K
MEDIUM	[24000, 24000, 24000, 24000]	96,000	0.001	150K
LARGE	[36000, 36000, 36000, 36000]	144,000	0.001	200K
DEEPER	[12000, 12000, 12000, 12000, 12000]	60,000	0.003	100K
VLARGE	[48000, 48000, 48000, 48000]	192,000	0.001	150K
HUGE	[128000, 128000, 128000, 128000]	512,000	0.001	200K

Post-hoc spectral profiling. After training and discretization, the aggregate spectral energy distribution across all neurons reveals whether the task genuinely exploits ternary structure. If most energy concentrates in linear Fourier terms (\hat{f}_{10} , \hat{f}_{01} , \hat{f}_{11}), the network is essentially performing sign propagation and could function as a Boolean circuit. If substantial energy appears in quadratic terms (\hat{f}_{20} , \hat{f}_{02} , \hat{f}_{22}), the network is genuinely exploiting the three-valued distinction, routing information differently based on whether inputs are decided versus undetermined. This spectral profile is a principled diagnostic for whether K_3 logic adds value over binary logic for a given task.

Vocabulary coverage. The Hamming distance between a neuron’s discretized truth table and the nearest curated gate quantifies vocabulary coverage. The Level 2 coverage (the fraction of neurons whose nearest curated gate has Hamming distance zero) reveals which tasks are “natively ternary” (high coverage) versus tasks requiring gates outside the standard vocabulary. One of the more interesting, formally defined vocabularies of ternary gates is that of *threshold logic* (Jones, 2012). In threshold logic, each input i_j is multiplied by a constant k_j and then the inputs are summed and then compared to two thresholds t_+ and t . If the sum is t_+ or greater, the output is +1. If the sum is t , the output is 1. According to Merrill Jr (1965), 471 of the 19,683 diadic ternary operators can be computed using threshold logic.

Appendix C. Additional Experimental Results

C.1. Supplementary: CIFAR-10 scaling details

C.1.1. TRAINING DYNAMICS

Base scales (48K-144K). Figure 4 shows training loss curves for four scales. At SMALL and MEDIUM scales, DLGN enters a noisy plateau (oscillating in 0.5-1.4), while PST achieves 10-38 \times lower task loss (e.g., TLGN-LARGE: 0.017 vs. DLGN-LARGE: 0.65). The 5-layer DEEPER variant shows the same plateau as SMALL, confirming that depth alone does not resolve it.

Extended scales (192K-512K). Figure 5 extends to VLARGE and HUGE. DLGN-HUGE (512K) breaks through to 0.015, a qualitative transition from plateau-dominated to clean convergence, suggesting the softmax-over-gates parameterization requires a threshold overparameterization level (between 48K and 128K per-layer width). TLGN-HUGE reaches 0.004, the lowest task loss of any model.

Ternary convergence. Figure 6 overlays TLGN task loss curves for VLARGE and HUGE. TLGN-HUGE reaches its floor ($\sim 10^{-3}$) by step 30K, matching TLGN-VLARGE’s asymptotic performance in

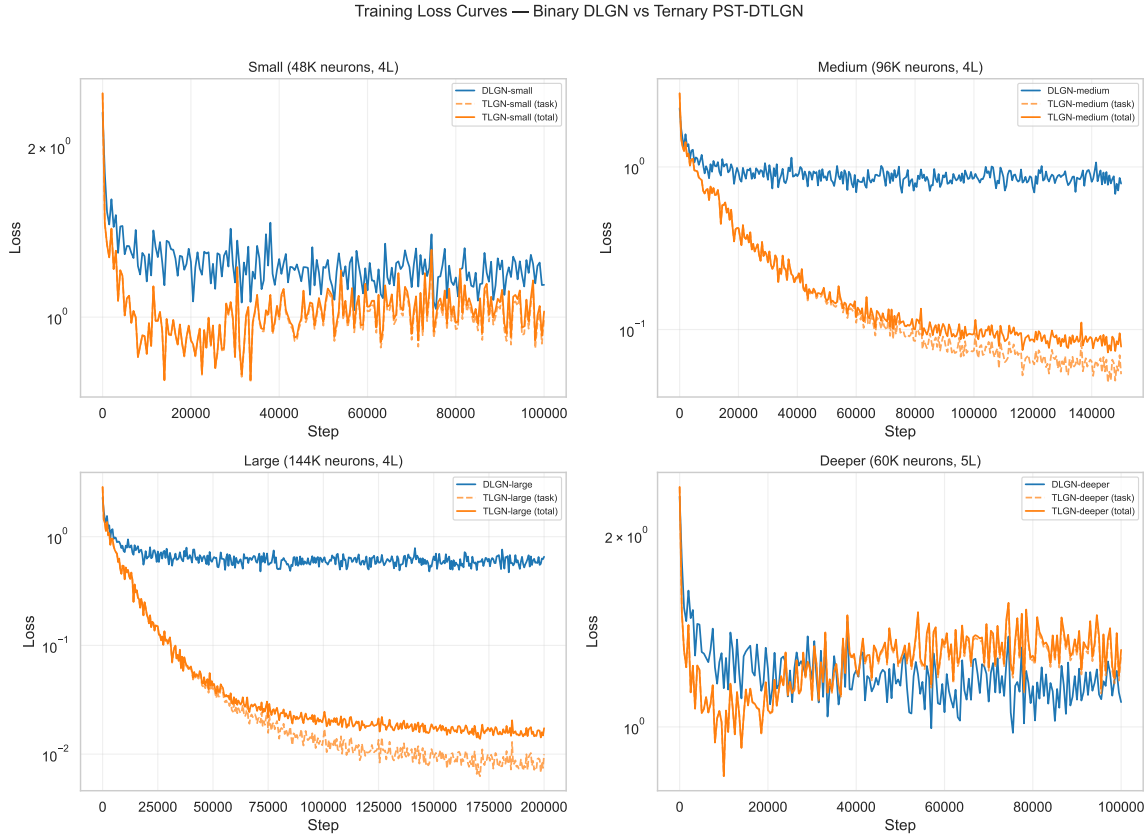


Figure 4: **Training loss curves (SMALL–LARGE + DEEPER)**. 2×2 grid, log-scale y-axis. Blue: DLGN. Dashed orange: TLGN task loss. Solid orange: TLGN total loss (task + λ · commitment). TLGN converges 1-2 orders of magnitude below DLGN at MEDIUM and LARGE scales, while both remain comparable at SMALL scale.

Table 4: **Training wall time** (single RTX 4090). Speed ratio = DLGN time / TLGN time.

Scale	Neurons	DLGN (s)	TLGN (s)	Speedup
SMALL	48K	241	156	1.5×
MEDIUM	96K	587	292	2.0×
LARGE	144K	1023	479	2.1×
DEEPER	60K	297	167	1.8×
VLARGE	192K	936	455	2.1×
HUGE	512K	4408	1401	3.1×

15% of the training budget. Periodic spikes coincide with lambda annealing ramp-up; these are transient (recovery within 1-2K steps) and do not affect final performance.

C.1.2. HARDENING GAP MECHANISM

Three regimes govern the gap trajectory.

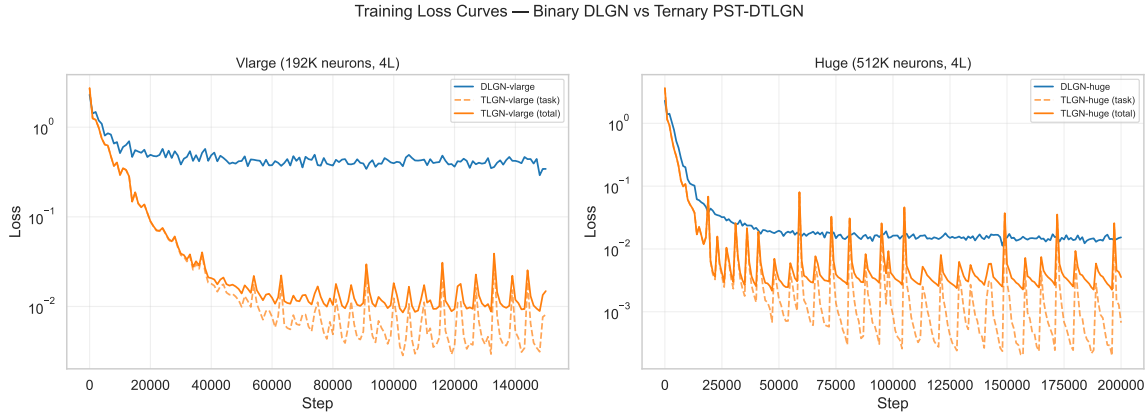


Figure 5: **Training loss curves (vLARGE and HUGE)**. Left: vLARGE (192K neurons). Right: HUGE (512K neurons). At HUGE scale, DLGN finally achieves clean convergence (0.015), eliminating the noisy-plateau pathology. TLGN-HUGE reaches 0.004 (task), the lowest of any model.

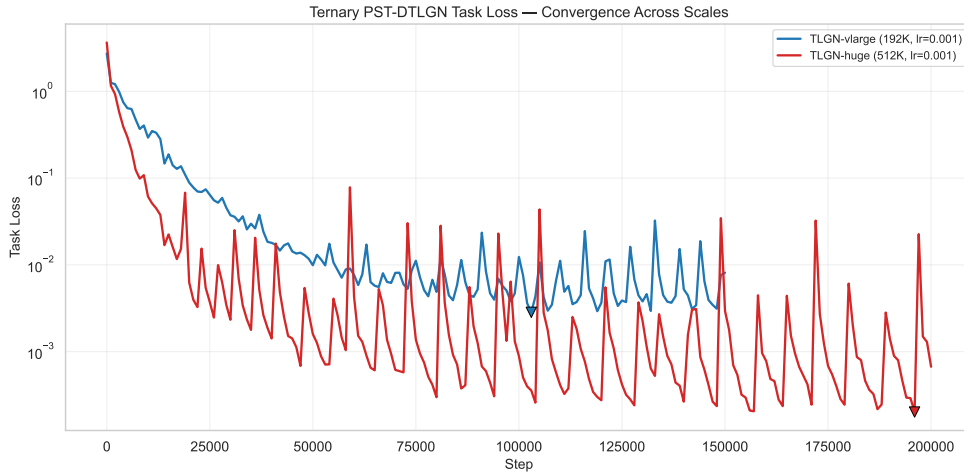


Figure 6: **Ternary task loss convergence (vLARGE and HUGE)**. Triangles mark the minimum. Both use lr=0.001. TLGN-HUGE reaches its floor ($\sim 10^{-3}$) by step 30K, matching TLGN-vLARGE’s asymptotic performance in 15% of the training budget, then continues improving to 3×10^{-4} . Periodic spikes (visible as upward excursions) coincide with lambda annealing ramp-up.

Regime I: Low capacity (48K-60K). Gap is modest (2.0-2.8 pp). The polynomials have limited freedom; the gap is small because there is little to lose in hardening. However, hardening error is high (0.298): the polynomials are not close to valid gates, but per-neuron rounding errors do not compound catastrophically at this scale.

Regime II: Mid capacity (96K-192K). Gap peaks at 14.1 pp (MEDIUM) and remains elevated through vLARGE (11.9 pp). The network develops rich polynomial representations far from valid ternary truth tables. The commitment regularizer reduces hardening error monotonically (0.253 \rightarrow 0.067), but accumulated rounding through four layers remains destructive.

Table 5: **Hardening error and UNKNOWN% across scales.** Hardening error drops 10× while UNKNOWN% increases 4× at HUGE scale.

Scale	TLGN Gap (pp)	Hard Err	UNK%
SMALL	+2.8	0.298	5.9%
DEEPER	+2.0	0.218	7.3%
MEDIUM	+14.1	0.253	6.2%
LARGE	+13.0	0.074	6.0%
VLARGE	+11.9	0.067	9.3%
HUGE	+3.7	0.029	24.6%

Table 6: **Gate diversity and functional redundancy.** Unique: distinct truth tables. Eff. Div: exponential Shannon entropy. Gini: concentration (higher = more concentrated). Max copies: neuron count of the most common gate. Singletons: gates used by exactly one neuron.

Model	Unique	Eff. Div	Gini	Redund.%	Max Copies	Singletons
DLGN-SMALL	16	14.9	0.176	100.0%	4,128	0
TLGN-SMALL	8,987	4,268	0.603	81.3%	224	3,149
DLGN-MEDIUM	16	14.7	0.209	100.0%	10,341	0
TLGN-MEDIUM	12,655	6,719	0.587	86.8%	144	3,032
DLGN-LARGE	16	14.5	0.222	100.0%	16,620	0
TLGN-LARGE	14,375	7,590	0.592	90.0%	190	2,578
DLGN-VLARGE	16	14.4	0.231	100.0%	23,263	0
TLGN-VLARGE	14,360	7,239	0.610	92.5%	338	2,181
DLGN-HUGE	16	14.2	0.251	100.0%	66,609	0
TLGN-HUGE	13,955	5,437	0.696	97.3%	1,490	1,710

Regime III: High capacity (512K). Gap contracts to 3.7 pp with hardening error 0.029, meaning each truth table entry is within 0.029 of the nearest ternary value on average. The contraction is accompanied by a sharp increase in UNKNOWN output neurons (24.6% vs. ~6% at smaller scales), reflecting implicit pruning: neurons near Voronoi cell boundaries in truth-table space are mapped to zero-output gates, while surviving neurons carry sufficient discriminative signal.

C.1.3. GATE DIVERSITY AND FOURIER SPECTRAL ANALYSIS

Table 6 reports gate diversity and functional redundancy. The effective diversity ratio (TLGN/DLGN) ranges from 286× (SMALL) to 523× (LARGE). Unique gates grow from 8,987 (SMALL) to ~14,000 (LARGE-VLARGE) then decrease slightly to 13,955 at HUGE, while Gini increases monotonically (0.603 → 0.696) and effective diversity drops from 7,590 to 5,437. The HUGE model uses fewer distinct gate types but copies each more frequently.

Table 7 decomposes the unique gates into Fourier complexity bands. Larger networks learn more complex gates: linear energy decreases from 36.8% (SMALL) to 32.6% (LARGE) while quadratic and cubic energy increase. The DEEPER variant has the most linear profile (37.7%), consistent with nar-

Table 7: **Fourier spectral profile** (TLGN models). Percentage of total Fourier energy in each degree band. %Ternary: fraction of unique gates that are genuinely ternary (not binary-equivalent).

Model	Unique	%Ternary	Const	Linear	Quad	Cubic	Quartic
TLGN-SMALL	8,987	98.6%	18.1%	36.8%	31.4%	11.0%	2.8%
TLGN-MEDIUM	12,655	99.3%	17.4%	33.5%	33.1%	12.6%	3.3%
TLGN-LARGE	14,375	99.4%	17.0%	32.6%	33.5%	13.4%	3.5%
TLGN-DEEPER	9,068	96.8%	23.6%	37.7%	26.8%	9.4%	2.5%

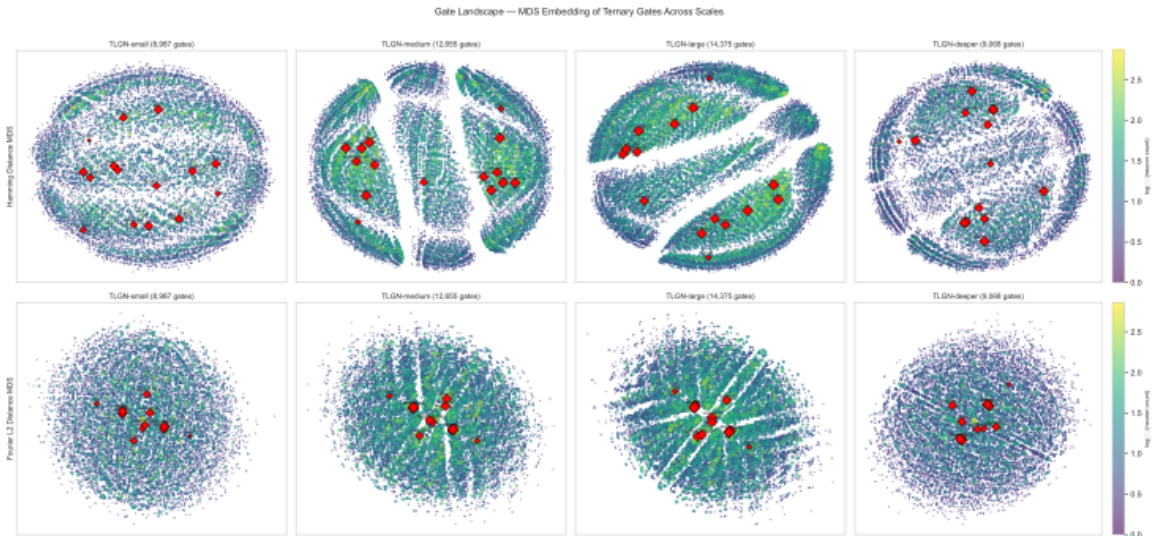


Figure 7: **Gate landscape - MDS embedding of ternary gates across scales.** Top row: Hamming distance (number of differing truth table entries out of 9). Bottom row: Fourier L^2 distance. Each point is a unique gate; area $\propto \log_2(\text{neuron count})$; colour encodes $\log_{10}(\text{neuron count})$. Red diamonds: the 15 named curated gates (AND, OR, XOR, etc.). Curated gates occupy the high-count core in all four embeddings, confirming that PST rediscovers classical logic operations without any gate-vocabulary constraint.

rower per-layer width limiting inter-neuron interaction complexity. Over 98% of gates are genuinely ternary at all scales.

C.1.4. GATE LANDSCAPE GEOMETRY VIA MDS EMBEDDING

The Fourier spectral profile (Table 7) summarizes *aggregate* complexity but does not reveal how the $\sim 9,000$ – $14,000$ unique gates are organized relative to one another. We apply multidimensional scaling (MDS) under two complementary distance metrics: Hamming distance on truth tables; and, Euclidean (L^2) distance on Fourier coefficient vectors; to embed each unique gate as a point in \mathbb{R}^2 . Figure 7 shows the result for all four base scales.

Clustering of learned gates around named gates. Under both metrics and at all four scales, the highest-count learned gates (bright points, $\log_{10}(\text{count}) > 2$) cluster in the same region as the 15 named curated gates (red diamonds). This co-location indicates that PST, despite searching an

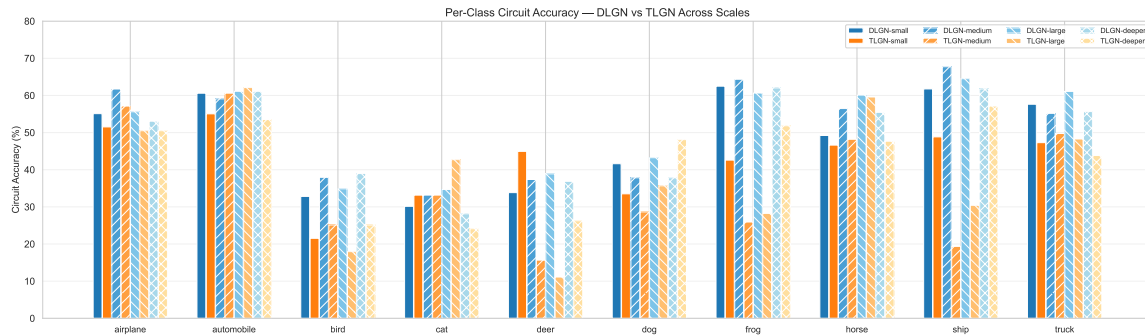


Figure 8: **Per-class circuit accuracy at smaller scales.** Blue: DLGN. Orange: TLGN. Solid: lower scale. Hatched: higher scale. TLGN shows high class-level variance at SMALL-DEEPER scales, with catastrophic failures on visually complex classes (bird, cat, deer, frog). For larger scales (VLARGE, HUGE) showing partial recovery, see Figure 2 in the main text.

unconstrained space of 19,683 truth tables, independently converges toward the neighbourhood of classical logic operations (AND, OR, XOR, NAND, etc.). Low-count gates — including the $\sim 2,600$ singletons at LARGE (Table 6) - are scattered at greater embedding distances from this core, consistent with their role as rare, task-specific functions.

The two metrics provide complementary views. Hamming distance captures how many truth table entries differ between gates (out of 9), so nearby points in the top row are *functionally* similar. Fourier L^2 distance captures differences in spectral energy distribution, so nearby points in the bottom row share similar complexity profiles regardless of which specific entries differ. The named gates occupy the high-count core under both metrics, confirming that they are central in both the functional and spectral sense.

Scale dependence. From SMALL to LARGE, the gate cloud grows denser as unique gates increase (8,987 \rightarrow 14,375) and effective diversity rises (4,268 \rightarrow 7,590; Table 6). The DEEPER variant (right-most column), despite a comparable neuron count to SMALL, produces a more compact cloud, consistent with its higher constant-energy fraction (23.6% vs. 18.1%) and lower quadratic-energy fraction (26.8% vs. 31.4%; Table 7).

C.1.5. PER-CLASS ANALYSIS

The per-class breakdown (Figure 8, Table 8) reveals that the TLGN hardening gap is not uniform across classes.

TLGN-HUGE recovers on hard classes. The most dramatic improvements from VLARGE to HUGE occur on visually complex classes: bird (+32.3 pp), cat (+37.2 pp), frog (+26.9 pp), and ship (+13.8 pp). At HUGE scale, TLGN surpasses DLGN on bird (50.8% vs. 43.6%) and cat (50.8% vs. 30.7%).

Dog class regression. TLGN-VLARGE achieved 64.3% on dog but TLGN-HUGE drops to 30.8% (-33.5 pp). The dog-cat confusability in CIFAR-10 and the $4\times$ increase in UNKNOWN neurons suggest a redistribution of discriminative capacity rather than uniform improvement.

DLGN is more uniform. Binary circuit accuracy has lower per-class variance (CoV: 0.23 for DLGN-HUGE vs. 0.28 for TLGN-HUGE) and dominates on “easy” classes (frog: 65.3% vs. 51.4%; automobile: 65.2% vs. 56.6%).

Table 8: **Per-class circuit accuracy (%) at selected scales.** Bold: best ternary result per class. Δ : improvement from VLARGE to HUGE. Classes with VLARGE accuracy $< 30\%$ are marked with †.

Class	TLGN				DLGN ref.		
	SMALL	LARGE	VLARGE	HUGE	VLARGE	HUGE	$\Delta_{vl \rightarrow h}$
airplane	51.5	50.5	62.8	61.2	58.7	60.2	-1.6
automobile	55.1	62.1	55.6	56.6	58.6	65.2	+1.0
bird†	21.5	17.9	18.5	50.8	37.9	43.6	+32.3
cat†	33.2	42.7	13.6	50.8	32.7	30.7	+37.2
deer†	44.9	11.1	24.2	25.8	36.4	40.9	+1.6
dog	33.5	35.7	64.3	30.8	44.9	44.9	-33.5
frog†	42.6	28.2	24.5	51.4	65.7	65.3	+26.9
horse	46.6	59.6	37.8	46.1	55.4	56.5	+8.3
ship	48.8	30.4	42.4	56.2	69.1	62.2	+13.8
truck	47.3	48.3	51.2	52.7	57.1	58.6	+1.5

Table 9: **Margin-based selective classification** (2K test samples). Margin(C/W): mean GroupSum margin for correct/wrong predictions. Separation: ratio of correct to wrong margin. Acc@ $k\%$: accuracy when retaining only the $k\%$ most confident samples.

Model	Circ Acc	Margin(C)	Margin(W)	Sep.	Acc@90%	Acc@50%
DLGN-SMALL	48.9%	37.1	19.5	1.90×	52.0%	64.3%
TLGN-SMALL	42.6%	38.4	22.9	1.68×	44.8%	54.5%
DLGN-LARGE	51.7%	49.3	26.6	1.85×	54.9%	66.1%
TLGN-LARGE	38.5%	66.3	41.3	1.61×	39.9%	48.3%
DLGN-VLARGE	52.0%	58.6	30.1	1.95×	54.6%	66.3%
TLGN-VLARGE	39.2%	85.6	51.9	1.65×	41.2%	49.5%
DLGN-HUGE	53.0%	106.4	50.5	2.11×	55.7%	70.3%
TLGN-HUGE	48.4%	131.7	73.9	1.78×	50.6%	61.5%

C.1.6. MARGIN-BASED CONFIDENCE

Ternary circuits provide a natural confidence signal via the GroupSum margin (difference between highest and second-highest class scores).

Ternary margins are larger in absolute magnitude ($\{-1, 0, 1\}$ outputs actively suppress competing classes), but DLGN achieves better margin *separation*: $2.11\times$ vs. $1.78\times$ at HUGE scale, yielding Acc@50% of 70.3% vs. 61.5%. Ternary separation improves with scale ($1.65\times \rightarrow 1.78\times$ from VLARGE to HUGE; Acc@50%: $49.5\% \rightarrow 61.5\%$), indicating genuine improvement in discriminative quality of surviving neurons.

C.2. Appendix: Supporting Experiments

C.2.1. DECISION BOUNDARY GALLERY

Figure 9 presents the full 5×4 decision boundary gallery. Each row shows one dataset; columns display the raw data, binary circuit boundary, ternary circuit boundary, and UNKNOWN density

Table 10: **Gaussian separation sweep.** As separation increases, UNKNOWN fraction tracks the Bayes error. Binary accuracy matches the Bayes rate at all separations, confirming neither architecture is capacity-limited.

Separation	Tern Acc	UNK%	Bin Acc	Bayes
0.5σ	59.8%	54.9%	68.2%	68.2%
1.0σ	71.0%	53.1%	83.5%	83.5%
1.5σ	78.7%	50.6%	90.5%	90.5%
2.0σ	85.5%	44.0%	97.8%	97.8%
2.5σ	92.2%	39.1%	99.0%	99.0%
3.0σ	93.5%	37.5%	99.8%	99.8%

Table 11: **Asymmetric thresholding sweep** (Moons, test set).

δ	Test Acc	UNK%	Gap
1.00	85.8%	52.8%	0.00%
0.50	95.0%	38.3%	0.00%
0.25	93.0%	36.6%	0.00%
0.00	91.7%	42.0%	-0.81%

overlay. Across all five datasets, the ternary UNKNOWN regions (orange) concentrate at decision boundaries, confirming the pattern described in Section 5.2.1.

The UNKNOWN fraction ranges from 38.3% (Ring Sector) to 52.9% (Moons), scaling with boundary complexity. Ring Sector, with its clean angular separation, produces the smallest UNKNOWN band; Moons, with its high boundary curvature and noise = 0.5, produces the largest.

C.2.2. ACCURACY VS. COVERAGE CURVES

Figure 10 shows the full accuracy-vs-coverage curves for three representative datasets. The monotonic increase confirms that the GroupSum margin is a well-calibrated confidence proxy: low-margin predictions are disproportionately incorrect, and abstaining on them systematically improves accuracy on the retained set.

C.2.3. CONTROLLING THE UNKNOWN BAND

The `delta_fraction` parameter ($\delta \in [0, 1]$) controls the width of the UNKNOWN encoding band. Table 11 and Figure 11 show that peak accuracy on Moons occurs at $\delta=0.50$ (95.0%), not at either extreme. Notably, UNK% does not reach zero even at $\delta=0.0$ (42.0%), because UNKNOWN outputs emerge from internal truth tables, not only from the input encoding.

C.2.4. ENCODING RESOLUTION

Higher resolution simultaneously increases accuracy and decreases UNKNOWN rate (Table 12, Figure 12): from 84.0% accuracy / 53.8% UNK at $K=2$ to 95.5% / 23.8% at $K=16$, confirming that the UNKNOWN band reflects input-level ambiguity resolvable by finer quantization.

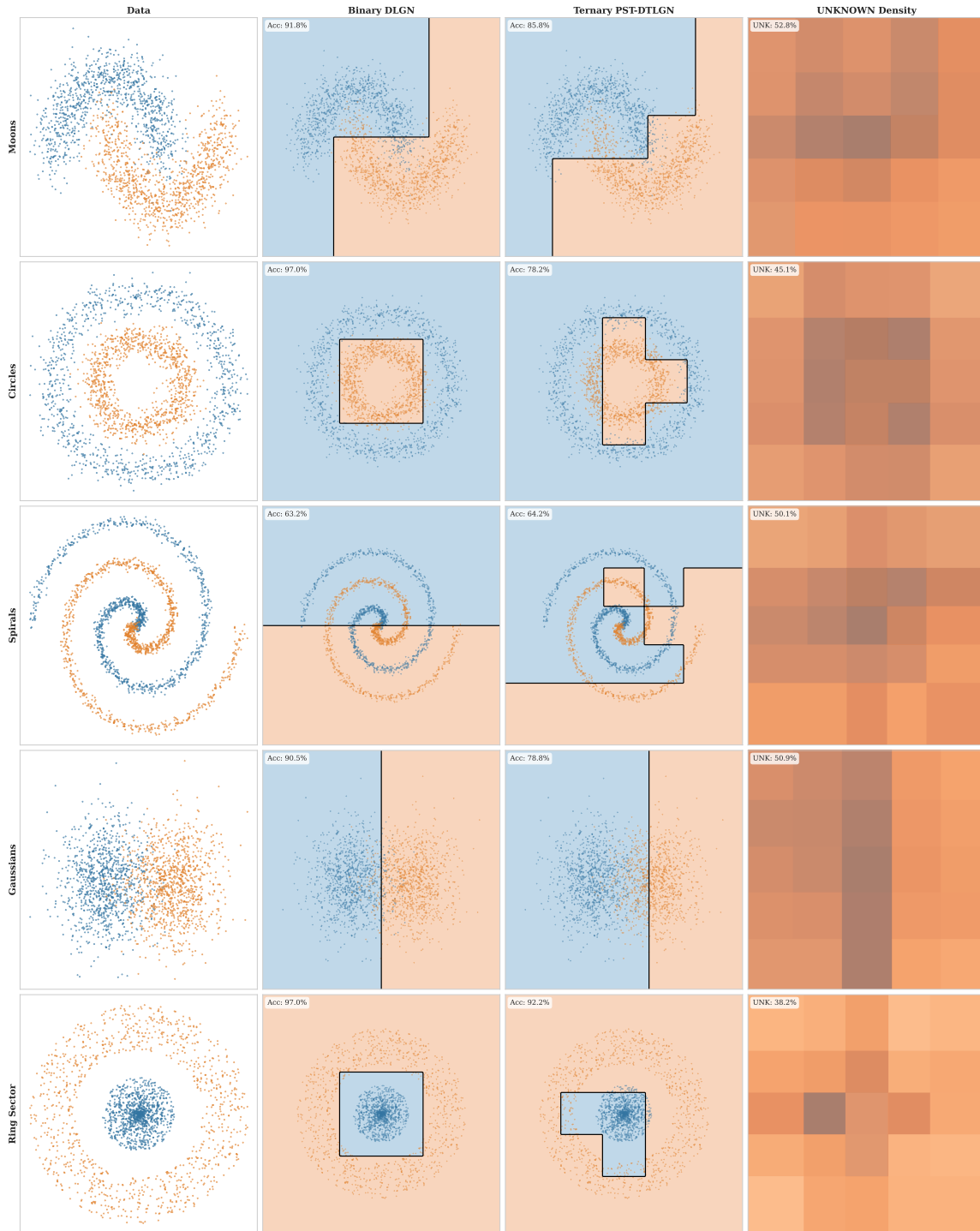


Figure 9: **Decision boundary gallery** (5×4 grid). Rows: Moons, Circles, Spirals, Gaussians, Ring Sector. Columns: raw data, binary boundary, ternary boundary, UNKNOWN density. Orange regions mark where $> 50\%$ of output neurons produce zero.

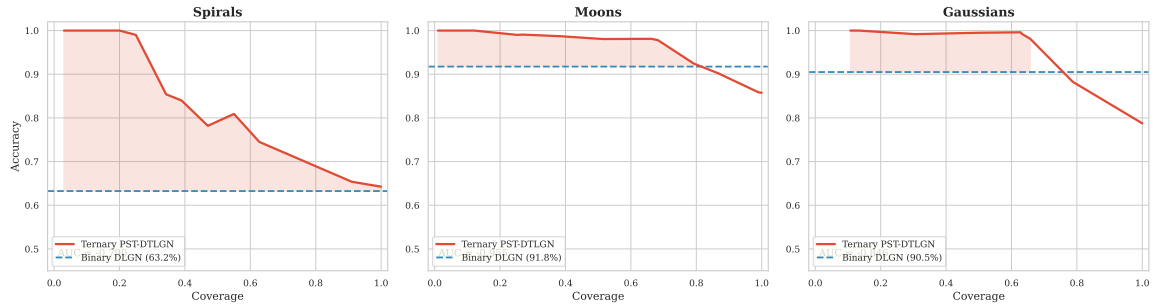


Figure 10: **Accuracy vs. coverage** (Spirals, Moons, Gaussians). As the circuit abstains on the lowest-margin samples, accuracy on the retained samples rises monotonically. The AUC quantifies selective prediction quality (closer to -1.0 is better).

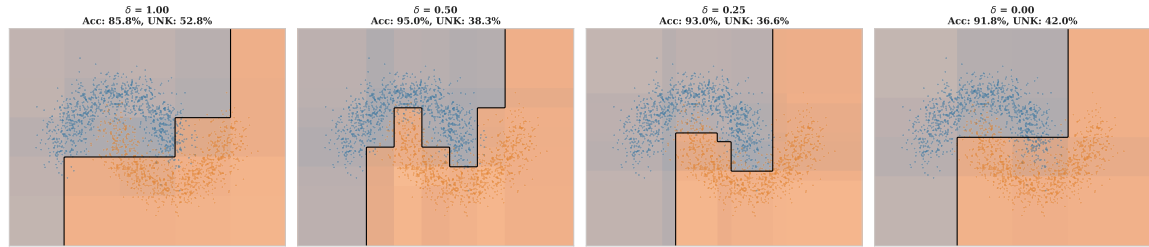


Figure 11: **Asymmetric thresholding** (Moons, four δ values). Peak accuracy (95.0%) at $\delta=0.50$, not at the binary-like extreme.

C.2.5. GATE DIVERSITY

PST discovers $\sim 1,200$ unique gates per dataset (out of 19,683), with effective diversity $\sim 1,050$, representing $70\times$ greater vocabulary utilization than binary’s fixed 16 (Table 13). Ternary redundancy is 28-31% vs. binary’s 99.1%, reflecting the two strategies: binary achieves expressiveness through dense repetition; ternary through gate specialization.

C.2.6. HARDENING GAP COMPARISON

Figure 13 compares the hardening gap across all datasets. Both architectures achieve small gaps under discrete-input training (binary $\leq 3.19\%$, ternary $\leq 8.31\%$). The near-zero ternary gaps on Moons (0.00%), Gaussians (0.31%), and Ring Sector (0.38%) validate the fidelity of the PST hardening procedure.

Appendix D. Polynomial Representations for Boolean Logic Functions

Let P_n denote the set of real multi-linear polynomials that represent Boolean functions over n variables. Given real multi-linear polynomials $p, q \in P_n$, define the binary operators meet (\wedge) and join (\vee):

$$p \wedge q := -\frac{1}{2} + \frac{1}{2}p(x) + \frac{1}{2}q(x) + \frac{1}{2}p(x)q(x), \quad p \vee q := \frac{1}{2} + \frac{1}{2}p(x) + \frac{1}{2}q(x) - \frac{1}{2}p(x)q(x),$$

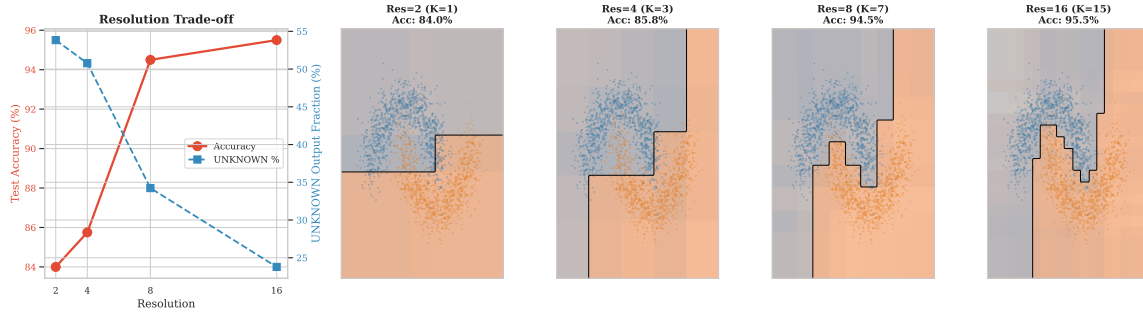


Figure 12: **Resolution vs. accuracy and UNKNOWN rate (Moons)**. Higher resolution increases accuracy and decreases UNKNOWN fraction.

Table 12: **Resolution sweep (Moons, test set)**.

K	Input Dim	Body Widths	Test Acc	UNK%
2	2	$[128]^3$	84.0%	53.8%
4	6	$[256]^3$	85.8%	50.8%
8	14	$[512]^3$	94.5%	34.2%
16	30	$[1024]^3$	95.5%	23.8%

and define the unary operator complementation (\neg):

$$\neg p := -p(x).$$

Then $(P_n, \vee, \wedge, \neg, \perp, \top)$ is a Boolean algebra with the top element being the constant polynomial $p(x) = 1$ and the bottom element being the constant polynomial $p(x) = -1$. For two-input Boolean functions ($n = 2$), the Boolean algebra of real multi-linear polynomials is generated by the set $\{x_1, x_2\}$, meaning one can reconstruct all Boolean functions using the operations meet, join, and complement applied to the set of generators.

D.1. The Boolean Group

The exclusive not-or¹ (XNOR) of elements in the Boolean algebra can be defined as:

$$p \odot q := p(x)q(x).$$

The structure (P_n, \odot, \top) is a finite abelian group, with the constant polynomial $p(x) = 1$ serving as the identity element and each element acting as its own inverse, $p \odot p = \top$. This subtle notion allows us to employ the results of Fourier analysis on finite groups (see: [Terras \(1999\)](#)). We restrict the remaining analysis to the case where $n = 2$. Define the character homomorphism $\mathcal{X} : P_2 \rightarrow \mathbb{R}$ as the trivial mapping $p \mapsto p(x)$ for $p \in P_2$, $x \in \{-1, 1\}^2$. Characters satisfy the condition

1. Typically a Boolean group derived from a Boolean algebra uses symmetric difference (exclusive or) for group multiplication. If we instead defined TRUE as -1 and FALSE as $+1$ (intepreted as the square roots of unity), then XOR would be the intuitive choice satisfying $p \oplus q := p(x)q(x)$.

Table 13: **Gate diversity** (both architectures, all datasets).

Dataset	Ternary			Binary		
	Unique	Eff. Div	Red.%	Unique	Eff. Div	Red.%
Moons	1,214	1,051.8	30.1%	16	15.3	99.1%
Circles	1,225	1,065.1	29.4%	16	15.6	99.1%
Spirals	1,224	1,062.2	29.5%	16	15.3	99.1%
Gaussians	1,201	1,037.9	30.8%	16	15.6	99.1%
Ring Sector	1,253	1,089.1	27.8%	16	15.8	99.1%

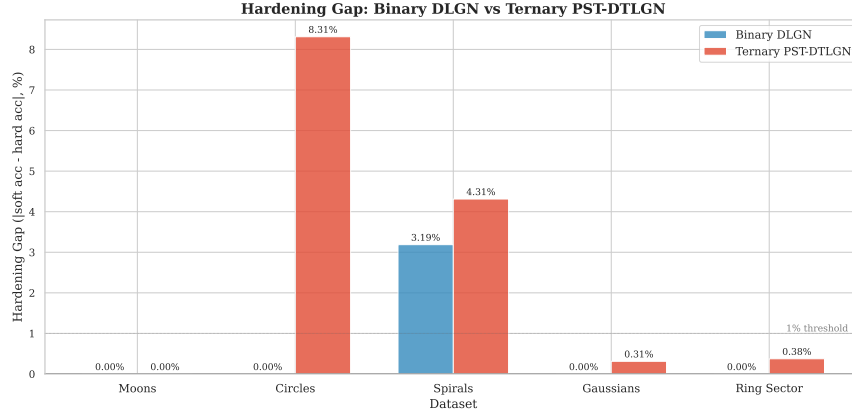


Figure 13: **Hardening gap** (all datasets). Both architectures achieve small gaps. The ternary gap is elevated on Circles and Spirals.

$\mathcal{X}(p \odot q) = \mathcal{X}(p)\mathcal{X}(q)$ for all $p, q \in P_2$. Define an inner product on the space of characters as:

$$\langle \varphi, \psi \rangle = \frac{1}{4} \sum_{x \in \{-1, 1\}^2} \varphi(x)\psi(x). \quad (\text{D.1})$$

We are interested in identifying orthonormal functions with respect to (D.1) that form the basis for all representations of Boolean functions. Consider the character functions $\{1, x_1, x_2, x_1x_2\} \subset \mathcal{X}(P_2)$. These functions form an orthonormal basis for the characters of P_2 . Enumerating the basis functions such that:

$$\varphi_0(x) = 1, \quad \varphi_1(x) = x_1, \quad \varphi_2(x) = x_2, \quad \varphi_3(x) = x_1x_2,$$

we have:

$$\langle \varphi_i, \varphi_j \rangle = \begin{cases} 1, & i = j, \\ 0, & i \neq j. \end{cases}$$

Furthermore, any $p \in P_2$, $\mathcal{X}(p)$ can be uniquely represented as a linear combination of these basis functions. Given $p \in P_2$, the Fourier coefficients are determined by:

$$w_i = \langle \mathcal{X}(p), \varphi_i \rangle,$$

and we have then:

$$p(x) = \sum_{i=1}^4 w_i \varphi_i(x).$$

